A multicell matrix solution to the Boltzmann equation applied to the anisotropic electron transport in silicon

2003 J. Phys. A: Math. Gen. 36 8759

(http://iopscience.iop.org/0305-4470/36/33/304)

INSTITUTE OF PHYSICS PUBLISHING JOURNAL OF PHYSICS A: MATHEMATICAL AND GENERAL

J. Phys. A: Math. Gen. **36** (2003) 8759–8774 PII: S0305-4470(03)63995-8

A multicell matrix solution to the Boltzmann equation applied to the anisotropic electron transport in silicon

C Ertler and F Schürrer

Institut für Theoretische Physik, Technische Universität Graz, Petersgasse 16, A-8010 Graz, Austria

E-mail: ertler@itp.tu-graz.ac.at and schuerrer@itp.tu-graz.ac.at

Received 28 May 2003
Published 5 August 2003
Online at stacks.iop.org/JPhysA/36/8759

Abstract

A new method for solving the Boltzmann transport equation is introduced. The method is based on a discontinuous spline approximation of the distribution function in the whole phase space. This procedure enables us to avoid the widely used P_N-approximation for the angle dependence of the distribution function, so that we are able to treat strong anisotropies. The method is applied to a nonparabolic multivalley model of silicon, which allows for the investigation of the anisotropic high field transport of electrons in n-type silicon. The results are compared to experimental data and Monte Carlo simulations.

PACS number: 02.30.Nm

1. Introduction

The Boltzmann transport equation (BTE) is an integro-differential equation, which can be solved rigorously only in simple cases. Therefore, many approximative methods, e.g., discrete velocity models, kinematic model-equations simplifying the complicated collision integral and multigroup approaches were developed in the past [1]. The latter method, originally devised for neutron transport, was recently generalized for nonlinear extended Boltzmann equations [2, 3]. However, this brings in additional unknowns which stem from the integration of the force term in the BTE. A continuous multigroup approach overcomes this difficulty [4] but numerical simulations show the emergence of oscillations correlated to the number of groups [5]. Moreover, the well-established procedure in the neutron transport theory of treating the angle dependence of the distribution function by a truncated expansion in spherical harmonics (P_N-approximation [6]) proves to be inappropriate in describing strong anisotropies caused by strong external forces. To compensate for these disadvantages, we propose a discontinuous multicell spline approximation describing the angle dependence in the same flexible way as it was already done for the energy dependence of the distribution function. Even though the

approach is discontinuous, it is possible to find a way based on physical grounds to evaluate the integrated force term correctly.

The basic idea of the method is to split up the phase space into tiny cells and to approximate locally the carrier distribution function within these cells by a linear combination of a suitable set of basis functions (splines). To gain enough equations for the newly introduced unknowns, one can integrate the BTE over each cell by using, in principle, any weight function. By choosing appropriate weights one can establish the correct balance of macroscopic quantities, e.g., particle density, in the model equations. From a mathematical point of view, the method is based on the idea of weighted residuals [7]. This leads to a matrix representation of the BTE, which can be easily solved by standard numerical techniques.

We apply this multicell matrix method to a problem of physical interest where anisotropy becomes important, namely the transport of electrons in silicon affected by high electric fields. Under such circumstances the widely used drift-diffusion models fail on account of their foundation in describing typical high field effects such as the drift velocity saturation or the appearance of negative differential resistivity. Therefore, a much more complicated semiclassical BTE must be applied [8].

In this field of activity, the BTE is nowadays solved with high accuracy by Monte Carlo (MC) simulations which include the full band structure of the semiconductor and realistic phonon dispersion curves [9, 10]. Of course, these simulations are time-consuming even on powerful computers. For the purpose of device simulations it would be of interest to have an alternative, as a faster solution method which may be less accurate than the MC calculations but which reproduces all important high-field effects. In the past different alternative approaches were presented such as the iterative technique [11, 12], the scattering matrix approach [13] or a direct matrix method [14] based on a complete discretization of the BTE in the reciprocal $\boldsymbol{k}$-space. Moreover, recently finite difference schemes were applied to the BTE [15, 16]. Our work is also intended to take a further step in developing deterministic solution methods to the BTE.

The paper is organized as follows. The underlying physical model is described in section 2. We introduce the multicell matrix method in detail in section 3 and we finally apply it to n-type silicon in section 4. The numerical results are compared with the MC simulations and measurements.

2. Physical model

In n-type silicon the electrons of the conduction band contribute mainly to the charge transport. Therefore, neglecting holes in the valence band, we use a standard multivalley model [17] for the band structure of silicon by considering six equivalent valleys lying around the six minima along the Δ-directions of the conduction band. For values of the wave vector $\boldsymbol{k}$ close to the minima of the conduction band, the isoenergetic surfaces are ellipsoids. This means that the dispersion relation of energy ε of the electrons in the principal axis system is given by

$$\varepsilon(\boldsymbol{k}) = \frac{\hbar^2}{2}\left[\frac{1}{m_\mathrm{t}}\left(k_x^2 + k_y^2\right) + \frac{k_z^2}{m_\mathrm{l}}\right] \tag{1}$$

where $\boldsymbol{k}$ is the wave vector, m_t and m_l, respectively, denote the transversal and longitudinal effective mass of the electrons and $\hbar$ is the common notation for the ratio of Plancks constant and 2π. Using the Herring–Vogt transformation [18]

$$k_i^* = T_{ij}k_j \tag{2}$$

with

$$(T_{ij}) = \begin{pmatrix} \left(\frac{m_0}{m_t}\right)^{1/2} & 0 & 0 \\ 0 & \left(\frac{m_0}{m_t}\right)^{1/2} & 0 \\ 0 & 0 & \left(\frac{m_0}{m_l}\right)^{1/2} \end{pmatrix} \tag{3}$$

which reduces the ellipsoidal equienergetic surfaces to spheres, the dispersion relation can be rewritten in the parabolic form as

$$\varepsilon(k) = \frac{\hbar^2}{2m_0} k^{*2} \tag{4}$$

with the free electron mass m_0. But in the case of high field transport, electrons with wavevectors $\boldsymbol{k}$ far from the minima of the conduction band also emerge and their energies ε deviate from the quadratic expression given in equation (1). A simple analytic way of introducing nonparabolicity is to use an energy-wave vector relation of the type

$$\gamma = \varepsilon(1 + \alpha\varepsilon) = \frac{\hbar^2}{2m_0} k^{*2} \tag{5}$$

where α is the nonparabolicity parameter. A comparison with full band structure calculations shows that equation (5) gives the correct density of states up to energies of about 2 eV [9]. The most drastic approximation of our simple band structure model is the negligence of other secondary minima located at the centre of the Brillouin zone and along $\langle 111 \rangle$ directions. However, this can be crudely justified by the hand-waving argument that they correspond to high energies of the order of eV.

By setting up a BTE for the time-dependent distribution function $f^i(\boldsymbol{k}, t)$ in each valley for the case of an external electric field $\boldsymbol{E}$, one gets the coupled system

$$\frac{\partial f^i}{\partial t} = -\frac{e\boldsymbol{E}}{\hbar} \cdot \frac{\partial f^i}{\partial \boldsymbol{k}} + C[f^i] + C_{\text{i.v.}}[f^i, f^j] \qquad i, j = 1, \ldots, 6 \tag{6}$$

where e is the charge of an electron. The collision operators $C[f^i]$ and $C_{\text{i.v.}}[f^i, f^j]$, respectively, describe the change of the distribution function due to intra and intervalley scattering processes. We assume the electrons to interact only with phonons; impurity scattering and electron–electron collisions are neglected by assuming a low donor concentration ($\approx 10^{13}$) and accordingly a low-density electron gas. Selection rules for phonon-assisted transitions [19, 20] in silicon allow only for acoustic intravalley scattering, *f*-scattering between perpendicular valleys with longitudinal acoustic (LA) and transversal optical (TO) phonons, and g-scattering between opposite valleys with longitudinal optical (LO) phonons. However, the MC simulations show that other 'forbidden' low-energy intervalley phonon transitions are necessary to improve the agreement with experiments when high-field transport is considered [21, 22]. The contradiction to selection rules is softened by the fact that they are only strictly valid at high symmetry points of the Brillouin zone.

Considering a nondegenerate electron gas allows us to approximate $1 - f$ by 1, which essentially simplifies the mathematics by making the collision operator linear. A typical collision operator then reads

$$C[f] = \frac{V}{8\pi^3} \left(\int P(\boldsymbol{k}', \boldsymbol{k}) f(\boldsymbol{k}') \, \mathrm{d}^3 k' - \int P(\boldsymbol{k}, \boldsymbol{k}') f(\boldsymbol{k}) \, \mathrm{d}^3 k' \right) \tag{7}$$

where $P(\boldsymbol{k}', \boldsymbol{k})$ is the transition rate from state $\boldsymbol{k}'$ to $\boldsymbol{k}$ and V the volume of the crystal. The time-dependent perturbation theory using the deformation potential approximation for the Hamiltonian of the electron–phonon system provides the following general expression

for the probability per unit time of a scattering event assisted by a phonon of wavevector $\boldsymbol{q}$, polarization ξ and energy $\hbar\omega_q$

$$P(\boldsymbol{k},\boldsymbol{k}') = \frac{\pi}{\rho V \omega_q}\binom{N_q}{N_q+1}\mathcal{G}|\Xi_{ij}q_j\xi_i|^2\delta[\varepsilon(\boldsymbol{k}')-\varepsilon(\boldsymbol{k})\mp\hbar\omega_q] \tag{8}$$

where the upper and lower symbols refer to absorption and emission of a phonon, respectively. Here, ρ denotes the mass density of the semiconductor, Ξ_{ij} is a tensor that describes the shift of the electron band per unit deformation of the crystal and $\mathcal{G}$ is an overlap integral of Bloch states. The phonon number N_q is in the following always assumed to be equal to its equilibrium value at the temperature of the crystal. Finally, the Dirac-Delta function $\delta[\varepsilon(\boldsymbol{k}')-\varepsilon(\boldsymbol{k})\mp\hbar\omega_q]$ guarantees the energy conservation. In the case of normal processes the overlap factor equals unity for exact plane waves or for waves formed with pure s states. When lower symmetries are involved such as p states in the case of cubic semiconductors, the overlap factor is less than unity and mainly depends on the angle between initial and final states $\boldsymbol{k}$ and $\boldsymbol{k}'$, measured from the centre of the Brillouin zone. This angle does not spread over a wide range in the case of intra and intervalley scattering and thus $\mathcal{G}$ is almost constant. By including this value in the coupling constant Ξ, we can generally set the overlap factor to unity. In what follows, we introduce several simplifications to equation (8) in the specific case of acoustic and optical phonon scattering.

Due to selection rules, intravalley scattering is only enabled by acoustic phonons. When high electric fields are considered, acoustic scattering can be treated as an elastic process, because the average electron energy is of the order of the optical-phonon energy, and optical phonons can assume the task of exchanging energy between the electrons and the crystal. Moreover, acoustic phonon scattering only involves phonons with wave vectors near the centre of the Brillouin zone and, therefore, one can use a linear dispersion relation

$$\omega_q = u_{\mathrm{l,t}}q \tag{9}$$

where $u_{\mathrm{l,t}}$ denotes the longitudinal and transversal sound velocity, respectively. We also approximate the equilibrium Bose–Einstein distribution by the equipartition expression

$$N_q \approx \frac{k_0 T}{\hbar\omega_q} - \frac{1}{2}. \tag{10}$$

Here, k_0 denotes the Boltzmann constant and T is the lattice temperature. In fact, equation (10) is valid when $\hbar\omega_q \ll k_0 T$, i.e. when the thermal energy is much larger than the energy of the phonon involved in the transition. In the case of cubic lattice symmetry, the deformation-potential tensor reduces to two independent components Ξ_d and Ξ_u [18]. Applying all these assumptions to equation (8), the sum of the transition probabilities per unit time of absorption and emission processes becomes

$$P_{\mathrm{l}}(\boldsymbol{k},\boldsymbol{k}') = \frac{2\pi k_0 T}{\hbar\rho V u_{\mathrm{l}}^2}(\Xi_d + \Xi_u\cos^2\theta)^2\delta[\varepsilon(\boldsymbol{k}')-\varepsilon(\boldsymbol{k})] \tag{11}$$

for longitudinal modes and

$$P_{\mathrm{t}}(\boldsymbol{k},\boldsymbol{k}') = \frac{2\pi k_0 T}{\hbar\rho V u_{\mathrm{l}}^2}(\Xi_u\sin\theta\cos\theta)^2\delta[\varepsilon(\boldsymbol{k}')-\varepsilon(\boldsymbol{k})] \tag{12}$$

for transverse modes, where θ is the angle between $\boldsymbol{q}$ and the longitudinal axis of the valley considered. The effect of anisotropy is not large [23], and longitudinal and transversal modes can be treated in a combined way by replacing u_{l} and u_{t} by an average value $u = (2u_{\mathrm{t}} + u_{\mathrm{l}})/3$ and by averaging over the angle θ, which leads to the isotropic expression

$$P(\boldsymbol{k},\boldsymbol{k}') = \frac{2\pi k_0 T\,\Xi_{\mathrm{l}}^2}{\hbar\rho V u^2}\delta[\varepsilon(\boldsymbol{k}')-\varepsilon(\boldsymbol{k})]. \tag{13}$$

Intervalley scattering is induced by both low wavelength acoustic phonons and optical-mode phonons. In both cases the energy of the involved phonon can be assumed constant $\hbar\omega_q = \hbar\omega_{\mathrm{op}}$, because the dispersion curves are quite flat. Consequently, acoustic intervalley scattering can be treated in the same way as optical phonon transitions. Starting from equation (8), the scattering probability for optical phonons in the simplest case can be written as

$$P(\boldsymbol{k}, \boldsymbol{k}') = \frac{\pi (D_t K)^2}{\rho V \omega_{\mathrm{op}}} \begin{pmatrix} N_{\mathrm{op}} \\ N_{\mathrm{op}} + 1 \end{pmatrix} \delta[\varepsilon(\boldsymbol{k}') - \varepsilon(\boldsymbol{k}) \mp \hbar\omega_{\mathrm{op}}] \tag{14}$$

by replacing $|\Xi_{ij} q_j \xi_i|^2$ with a squared optical coupling constant $(D_t K)^2$. The phonon number N_{op} is given by the Bose–Einstein function evaluated at the constant phonon energy.

3. The multicell matrix method

Due to the simple form of the dispersion relation after applying the Herring–Vogt transformation [18], it is advantageous to set up each of the six BTEs (6) in its corresponding principal axis system and transform it afterwards to the 'starred system'. The transformed electric field $\boldsymbol{E}^{*(i)}$, $(i = 1, \ldots, 6)$, provides a certain direction in space. Thus, we can assume the distribution function $f^i(\boldsymbol{k}^*, t)$ to be symmetric around $\boldsymbol{E}^{*(i)}$ and, in this way, it only depends on the energy ε and $\chi^{(i)}$, the cosine of the angle between $\boldsymbol{k}^*$ and $\boldsymbol{E}^{*(i)}$. In the interest of less cumbersome notation, in future references to the single-valley quantities the superscript (i) will be dropped except where this would lead to ambiguity. The density of states (DOS) per valley is defined by

$$\mathcal{D}(\varepsilon) = \frac{1}{V} \sum_{\boldsymbol{k}', \uparrow + \downarrow} \delta[\varepsilon(\boldsymbol{k}') - \varepsilon(\boldsymbol{k})] \tag{15}$$

where the subscript $\uparrow + \downarrow$ means one must sum over both spin orientations. Using the nonparabolic dispersion relation (5), this leads to

$$\mathcal{D}(\varepsilon) = \frac{\sqrt{2} m_d^{3/2}}{\pi^2 \hbar^3} \gamma^{1/2} (1 + 2\alpha\varepsilon) \tag{16}$$

where the 'DOS-effective mass' $m_d = \left(m_t^2 m_l\right)^{1/3}$ is introduced. It proves convenient to absorb the DOS-factor $\gamma^{1/2}(1 + 2\alpha\varepsilon)$ in the definition of the distribution function

$$\psi(\varepsilon, \chi, t) = \gamma^{1/2} (1 + 2\alpha\varepsilon) f(\varepsilon, \chi, t). \tag{17}$$

The system of BTEs (6) now reads

$$\frac{\partial \psi^i}{\partial t} = -\left(\frac{\partial \psi^i}{\partial t}\right)_{\boldsymbol{E}} + C_{\mathrm{ac}}[\psi^i] + C_{\mathrm{i.v.}}[\psi^i, \psi^j] \qquad i, j = 1, \ldots, 6 \quad j \neq i \tag{18}$$

where the force term

$$\left(\frac{\partial \psi^i}{\partial t}\right)_{\boldsymbol{E}} = \frac{e\boldsymbol{E}}{\hbar} \cdot \frac{\partial f^i}{\partial \boldsymbol{k}} \gamma^{1/2} (1 + 2\alpha\varepsilon) \tag{19}$$

after some algebra results in

$$\left(\frac{\partial \psi^i}{\partial t}\right)_{\boldsymbol{E}} = \alpha_{E^*} \left\{ \chi \left[\frac{\gamma^{1/2}}{1 + 2\alpha\varepsilon} \frac{\partial \psi}{\partial \varepsilon} - \psi \left(\frac{1}{2\gamma^{1/2}} + \frac{2\alpha\gamma^{1/2}}{(1 + 2\alpha\varepsilon)^2} \right) \right] + \frac{(1 - \chi^2)}{2\gamma^{1/2}} \frac{\partial \psi}{\partial \chi} \right\} \tag{20}$$

with $\alpha_{E^*} = \sqrt{2} e E^* / m_0^{1/2}$. By using the isotropic transition probability (13), the collision integral due to acoustic intravalley scattering yields

$$C_{\mathrm{ac}}[\psi^i(\varepsilon, \chi)] = \alpha_{\mathrm{ac}} \gamma^{1/2} (1 + 2\alpha\varepsilon) \left[\left(\frac{1}{2} \int_{-1}^{1} \psi(\varepsilon, \chi') \, \mathrm{d}\chi' \right) - \psi(\varepsilon, \chi) \right] \tag{21}$$

with the constant factor

$$\alpha_{\mathrm{ac}} = \frac{\sqrt{2}k_0 T\,\Xi_1^2 m_d^{3/2}}{\pi\rho u^2\hbar^4}. \tag{22}$$

Analogously, integrating the transition probability (14) by considering N_f different f-type phonons with energies $\hbar\omega_f^n$, $(n = 1, \ldots, N_f)$, and N_g g-type phonons with energies $\hbar\omega_{\mathrm{g}}^n$, $(n = 1, \ldots, N_g)$, the collision term due to f and g-type intervalley scattering finally reads

$$\begin{aligned} C_{\mathrm{i.v.}}^{\mathrm{g},f}[\psi^i(\varepsilon,\chi),\psi^j] = \sum_{j\neq i}\sum_{n=1}^{N_g,N_f}\alpha_{\mathrm{g},f}^n\Bigg\{\Bigg[\frac{1}{2}g(\varepsilon)\int_{-1}^{1}\psi^j\left(\varepsilon-\hbar\omega_{\mathrm{g},f}^n,\chi'\right) \\ + \exp\left(x_{\mathrm{g},f}^n\right)\psi^j\left(\varepsilon+\hbar\omega_{\mathrm{g},f}^n,\chi'\right)\mathrm{d}\chi'\Bigg] - \psi^i(\varepsilon,\chi)\Big[g\left(\varepsilon+\hbar\omega_{\mathrm{g},f}^n\right) \\ + \exp\left(x_{\mathrm{g},f}^n\right)g\left(\varepsilon-\hbar\omega_{\mathrm{g},f}^n\right)\Big]\Bigg\} \end{aligned} \tag{23}$$

where the summation with respect to j runs over perpendicular valleys in the case of f-scattering and for g-scattering j refers to the valley opposite to the considered valley i. Here, we have introduced the abbreviations $g(\varepsilon) = \gamma(\varepsilon)^{1/2}(1+2\alpha\varepsilon)$, $x_{\mathrm{g},f}^n = \hbar\omega_{\mathrm{g},f}^n/k_0T$ and

$$\alpha_{\mathrm{g},f}^n = \frac{m_d^{3/2}(D_t K)_{n,\mathrm{g},f}^2}{\sqrt{2}\pi\rho\hbar^3\omega_{\mathrm{g},f}^n}\frac{1}{\exp\left(x_{\mathrm{g},f}^n\right)-1}. \tag{24}$$

The basic idea of our method is to split the domain of definition of the distribution function ψ into tiny cells of rectangular form . This means that we introduce a huge number N_ε of energy groups of constant length Δ_ε defined by the intervals $I_\nu = [\varepsilon_{\nu-1}, \varepsilon_\nu]$ with $\varepsilon_\nu = \nu\Delta_\varepsilon$ and $\nu = 1, \ldots, N_\varepsilon$. Analogously, the χ-space which equals the interval $[-1, 1]$ is divided into N_χ groups $I_\mu = [\chi_{\mu-1}, \chi_\mu]$ of constant length $\Delta_\chi = 2/N_\chi$ with $\chi_\mu = \Delta_\chi\mu - 1$ and $\mu = 1, \ldots, N_\chi$. The distribution function is approximated over such a cell $B_{\nu\mu} = I_\nu \times I_\mu$ by a linear combination of modified Legendre polynomials

$$P_\nu^\lambda(\varepsilon) = \sqrt{\frac{2}{\Delta_\varepsilon}}P^\lambda(x_\nu) \qquad P_\mu^{\lambda'}(\chi) = \sqrt{\frac{2}{\Delta_\chi}}P^{\lambda'}(x_\mu) \tag{25}$$

where $P^{\lambda,\lambda'}$ denotes the Legendre polynomial of order λ, λ' and

$$x_\nu = 2\left(\frac{\varepsilon}{\Delta_\varepsilon} - \nu\right) + 1 \qquad x_\mu = 2\left(\frac{\chi+1}{\Delta_\chi} - \mu\right) + 1. \tag{26}$$

The modification (25) of the Legendre polynomial is motivated by obtaining in this way the useful orthogonality relations

$$\int_{I_\nu} P_\nu^\lambda P_\nu^l\,\mathrm{d}\varepsilon = \frac{2\delta_{\lambda l}}{2l+1} \qquad \int_{I_\mu} P_\mu^{\lambda'} P_\mu^l\,\mathrm{d}\chi = \frac{2\delta_{\lambda' l}}{2l+1} \tag{27}$$

where $\delta_{\lambda l}$ is the common Kronecker delta. Now, the distribution function reads

$$\psi(\varepsilon,\chi,t) \approx \sum_{\nu=1}^{N_\varepsilon}\sum_{\mu=1}^{N_\chi}\theta(B_{\nu\mu})\sum_{\lambda=0}^{\Lambda_\varepsilon}\sum_{\lambda'=0}^{\Lambda_\chi}\psi_{\nu\mu}^{\lambda\lambda'}(t)P_\nu^\lambda(\varepsilon)P_\mu^{\lambda'}(\chi) \tag{28}$$

where we have introduced the characteristic function

$$\theta(B_{\nu\mu}) = \begin{cases} 1 & \text{for } (\varepsilon,\chi) \text{ in } B_{\nu\mu} \\ 0 & \text{elsewhere} \end{cases} \tag{29}$$

and the unknowns $\psi_{\nu\mu}^{\lambda\lambda'}$, which depend on time t; $\Lambda_\varepsilon, \Lambda_\chi$ represent the truncation indices.

To determine these unknowns, we set up a system of moment equations by multiplying the BTE (6) by the weight functions $P_\nu^l P_\mu^{l'}$ for $l = 1, \ldots, \Lambda_\varepsilon$ and $l' = 1, \ldots, \Lambda_\chi$ and integrating it over the cells $B_{\nu\mu}$ for $\nu = 1, \ldots, N_\varepsilon$ and $\mu = 1, \ldots, N_\chi$. In this way, by using the orthogonality relations (27) one obtains

$$\int_{B_{\nu\mu}} \frac{\partial \psi}{\partial t} P_\nu^l P_\mu^{l'} \,\mathrm{d}\varepsilon \,\mathrm{d}\chi = \frac{4}{(2l+1)(2l'+1)} \frac{\partial \psi_{\nu\mu}^{ll'}}{\partial t}. \tag{30}$$

The integration of the collision operator for acoustic phonons (21) results in

$$\int_{B_{\nu\mu}} C_{\mathrm{ac}}[\psi] P_\nu^l P_\mu^{l'} \,\mathrm{d}\varepsilon \,\mathrm{d}\chi = \alpha_{\mathrm{ac}} \sum_{\lambda=0}^{\Lambda_\varepsilon} c_{\nu\lambda l} \left(\Delta_\chi \delta_{l'0} \sum_{\mu=1}^{N_\chi} \psi_{\lambda 0}^{\nu\mu} - \frac{2}{2l'+1} \psi_{\lambda l'}^{\nu\mu} \right) \tag{31}$$

with the constant

$$c_{\nu\lambda l} = \int_{-1}^{1} P^\lambda(x_\nu) \gamma^{1/2} (1 + 2\alpha\varepsilon) P^l(x_\nu) \,\mathrm{d}x_\nu. \tag{32}$$

In the following, the limits of the summation indices are dropped, where this is possible without misunderstanding.

If we assume that the energies of the intervalley phonons can be written as a multiple of the energy discretization interval Δ_ε, electrons of a certain valley i can only 'jump' from one cell into another, which belongs to a different valley j. Considering such a typical process assisted by a certain intervalley phonon with energy $\hbar\omega_{\mathrm{i.v.}} \approx s\Delta_\varepsilon$, the corresponding collision integral coincides with a single term of the sum (23). Integrating it over the cell $B_{\nu\mu}$ leads to

$$\begin{aligned} \int_{B_{\nu\mu}} C_{\mathrm{i.v.}}[\psi^i, \psi^j] P_\nu^l P_\mu^{l'} \,\mathrm{d}\varepsilon \,\mathrm{d}\chi = \alpha_{\mathrm{i.v.}} \Bigg[& \Delta_\chi \delta_{l'0} \sum_\mu \sum_\lambda c_{\nu\lambda l} \left(\mathrm{e}^{x_0} \psi_{\lambda 0}^{(j)\nu+s\mu} + \psi_{\lambda 0}^{(j)\nu-s\mu} \right) \\ & - \frac{2}{2l'+1} \sum_\lambda \psi_{\lambda l'}^{(i)\nu\mu} (c_{\nu+s\lambda l} + \mathrm{e}^{x_0} c_{\nu-s\lambda l}) \Bigg] \end{aligned} \tag{33}$$

where $x_0 = \hbar\omega_{\mathrm{i.v.}}/k_0T$ and $\alpha_{\mathrm{i.v.}}$ is given by equation (24) by changing corresponding subscripts. The emission of a phonon is not possible if the energy of the electrons is smaller than the phonon energy ($\varepsilon < \hbar\omega_{\mathrm{i.v.}}$). In order to conserve the particle number, we also demand that no electrons are up-scattered to energies higher than the maximum value $\varepsilon_{N_\varepsilon}$, which means that absorption of phonons is forbidden if $\varepsilon > \varepsilon_{N_\varepsilon} - \hbar\omega_{\mathrm{i.v.}}$. Therefore, if $\nu \leqslant s$ or $\nu > N_\varepsilon - s$ all terms in equation (33) with indices $\nu - s$ and $\nu + s$, respectively, must be cancelled.

The integration of the force term (20) yields

$$\begin{aligned} \int_{B_{\nu\mu}} \left(\frac{\partial \psi}{\partial t} \right)_E P_\nu^l P_\mu^{l'} \,\mathrm{d}\varepsilon \,\mathrm{d}\chi = \alpha_{E^*} \Bigg\{ & \int_{I_\mu} P_\mu^{l'} \chi \left[\psi \frac{\gamma^{1/2}}{1+2\alpha\varepsilon} P_\nu^l \right]_{\varepsilon_{\nu-1}}^{\varepsilon_\nu} \mathrm{d}\chi \\ & - \int_{B_{\nu\mu}} \chi \frac{\gamma^{1/2}}{1+2\alpha\varepsilon} \frac{\mathrm{d}P_\nu^l}{\mathrm{d}\varepsilon} \psi P_\mu^{l'} \mathrm{d}\varepsilon \,\mathrm{d}\chi + \int_{I_\nu} P_\nu^l \frac{1}{2\gamma^{1/2}} \left[\psi (1-\chi^2) P_\mu^{l'} \right]_{\chi_{\mu-1}}^{\chi_\mu} \mathrm{d}\varepsilon \\ & - \int_{B_{\nu\mu}} (1-\chi^2) \frac{1}{2\gamma^{1/2}} \frac{\mathrm{d}P_\mu^{l'}}{\mathrm{d}\chi} \psi P_\nu^l \,\mathrm{d}\varepsilon \,\mathrm{d}\chi \Bigg\}. \end{aligned} \tag{34}$$

Here, the problem arises as to how we must evaluate the distribution function at the boundaries of the cell $B_{\nu\mu}$. Since continuity of the distribution function is not guaranteed

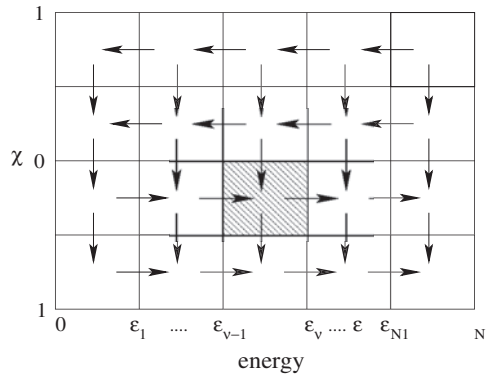

Figure 1. Possible jumps of electrons between cells according to the impact of an electric field.

by our ansatz (28), it makes a difference from which side one approaches the boundary. The right choice can be found on physical grounds. In the special case of $l = l' = 0$, the integral $\int_{B_{\nu\mu}} \psi P_\nu^0 P_\mu^0 \,\mathrm{d}\varepsilon \,\mathrm{d}\chi$ equals the particle density $n_{\nu\mu}$ in the cell $B_{\nu\mu}$ except for a constant factor. Hence, the corresponding moment equation can be interpreted as a continuity equation for the considered cell. Such an equation can also be derived from a heuristic point of view. The impact of an electric field on an electron in the state $\boldsymbol{k}$ can be described by the Pseudo-Newtonian law

$$\hbar \frac{\mathrm{d}\boldsymbol{k}}{\mathrm{d}t} = e\boldsymbol{E}. \tag{35}$$

Applying the Herring–Vogt transformation on equation (35) and rewriting the resulting vector equation in a special coordinate system, where the electric field vector coincides with the z-axis, one obtains

$$\frac{\mathrm{d}k_x^*}{\mathrm{d}t} = \frac{\mathrm{d}k_y^*}{\mathrm{d}t} = 0 \qquad \hbar \frac{\mathrm{d}k_z^*}{\mathrm{d}t} = eE^*. \tag{36}$$

Electrons are negatively charged and, therefore, the force acts along the negative z-axis. Integration of the equations of motion (36) shows that the x- and y-components of the wave vector remain constant, whereas the z-component tends to minus infinity with time. The modulus of the wave vector is proportional to the energy of the electron and χ denotes the cosine of the angle between $\boldsymbol{k}^*$ and $\boldsymbol{E}^*$. This means that if the electron starts with a positive k_z or equally $\chi > 0$, the energy first decreases until $\chi = 0$ and then increases to infinity. This implies, by limiting the maximum energy to $\varepsilon_{N_\varepsilon}$, that electrons, which are influenced by an electric field, can only jump between cells according to the scheme shown in figure 1. Considering now a cell $B_{\nu\mu}$ with the property $\chi < 0$, the particle density $n_{\nu\mu}$ of the cell changes in the time interval Δt by

$$\Delta n_{\nu\mu} = -n_{\nu\mu}\langle\dot{\chi}\rangle_{\nu\mu}\Delta t + n_{\nu\mu+1}\langle\dot{\chi}\rangle_{\nu\mu+1}\Delta t - n_{\nu\mu}\langle\dot{\varepsilon}\rangle_{\nu\mu}\Delta t + n_{\nu-1\mu}\langle\dot{\varepsilon}\rangle_{\nu-1\mu}\Delta t \tag{37}$$

where $\langle\cdot\rangle_{\nu\mu}$ denotes an averaging at the boundaries of the cell $B_{\nu\mu}$ and the dot marks the usual abbreviation for the derivative with respect to time. Since $k_z^* = \left(\sqrt{2}m_0^{1/2}/\hbar\right)\gamma^{1/2}\chi$ equation (36) leads to

$$\frac{\mathrm{d}k_z^*}{\mathrm{d}t} = \frac{m_0^{1/2}(1+2\alpha\varepsilon)}{\hbar\sqrt{2}\gamma^{1/2}\chi}\frac{\mathrm{d}\varepsilon}{\mathrm{d}t} + \frac{\sqrt{2}m_0^{1/2}\gamma^{1/2}}{\hbar(1-\chi^2)}\frac{\mathrm{d}\chi}{\mathrm{d}t} = eE^* \tag{38}$$

and by assuming either ε or χ to be constant, this provides

$$\dot{\chi} = \frac{\hbar(1-\chi^2)eE^*}{\sqrt{2}m_0^{1/2}\gamma^{1/2}} \qquad \dot{\varepsilon} = \frac{\hbar\sqrt{2}eE^*\gamma^{1/2}\chi}{m_0^{1/2}(1+2\alpha\varepsilon)}. \tag{39}$$

After calculating the averages

$$\begin{aligned}\langle\dot{\varepsilon}\rangle_{\nu\mu} &= \frac{1}{n_{\nu\mu}V}\sum_{\substack{\varepsilon=\varepsilon_\nu,\chi\in I_\mu\\ \uparrow+\downarrow}}\dot{\varepsilon}\,f(\varepsilon,\chi)\\ \langle\dot{\chi}\rangle_{\nu\mu} &= \frac{1}{n_{\nu\mu}V}\sum_{\substack{\chi=\chi_{\mu-1},\varepsilon\in I_\nu\\ \uparrow+\downarrow}}\dot{\chi}\,f(\varepsilon,\chi)\end{aligned} \tag{40}$$

and carrying out the limit $\Delta t \to 0$ equation (37) finally yields

$$\begin{aligned}\frac{\partial n_{\nu\mu}}{\partial t} = \alpha_{E^*}\frac{m_d^{3/2}}{\sqrt{2}\hbar^2\pi^2}\Bigg\{&\int_{I_\nu}\frac{1}{2\gamma^{1/2}}\left[-\left(1-\chi_{\mu-1}^2\right)\psi\left(\varepsilon,\chi_{\mu-1}^+\right)+\left(1-\chi_\mu^2\right)\psi\left(\varepsilon,\chi_\mu^+\right)\right]\mathrm{d}\varepsilon\\ &+\int_{I_\mu}\chi\left[\frac{\gamma(\varepsilon_\nu)^{1/2}}{1+2\alpha\varepsilon_\nu}\psi(\varepsilon_\nu^-,\chi)-\frac{\gamma(\varepsilon_{\nu-1})^{1/2}}{1+2\alpha\varepsilon_{\nu-1}}\psi(\varepsilon_{\nu-1}^-)\right]\mathrm{d}\chi\Bigg\}\end{aligned} \tag{41}$$

where the superscripts $+/-$ denote the right and left side limit, respectively. In the case of $\chi > 0$ one obtains by an analogous derivation

$$\begin{aligned}\frac{\partial n_{\nu\mu}}{\partial t} = \alpha_{E^*}\frac{m_d^{3/2}}{\sqrt{2}\hbar^2\pi^2}\Bigg\{&\int_{I_\nu}\frac{1}{2\gamma^{1/2}}\left[-\left(1-\chi_{\mu-1}^2\right)\psi\left(\varepsilon,\chi_{\mu-1}^+\right)+\left(1-\chi_\mu^2\right)\psi\left(\varepsilon,\chi_\mu^+\right)\right]\mathrm{d}\varepsilon\\ &+\int_{I_\mu}\chi\left[-\frac{\gamma(\varepsilon_{\nu-1})^{1/2}}{1+2\alpha\varepsilon_{\nu-1}}\psi\left(\varepsilon_{\nu-1}^+,\chi\right)+\frac{\gamma(\varepsilon_\nu)^{1/2}}{1+2\alpha\varepsilon_\nu}\psi\left(\varepsilon_\nu^+\right)\right]\mathrm{d}\chi\Bigg\}.\end{aligned} \tag{42}$$

Now, equation (34) can be easily evaluated by comparing it to the heuristically gained equations (41) and (42), which results in

$$\begin{aligned}\int_{B_{\nu\mu}}\left(\frac{\partial\psi}{\partial t}\right)_{\boldsymbol{E}}P_\nu^l P_\mu^{l'}\mathrm{d}\varepsilon\,\mathrm{d}\chi = \alpha_{E^*}\Bigg\{&\frac{2}{\Delta_\varepsilon}\sum_{\lambda\lambda'}(-1)^\lambda C^1_{\mu\lambda' l'}\left[\psi_{\lambda\lambda'}^{\nu+1\mu}\beta(\varepsilon_\nu)-\psi_{\lambda\lambda'}^{\nu\mu}(-1)^l\beta(\varepsilon_{\nu-1})\right]\\ &+\frac{2}{\Delta_\chi}\sum_{\lambda\lambda'}(-1)^{\lambda'}C^3_{\nu\lambda l}\left[\psi_{\lambda\lambda'}^{\nu\mu+1}\left(1-\chi_\mu^2\right)-\psi_{\lambda\lambda'}^{\nu\mu}(-1)^{l'}\left(1-\chi_{\mu-1}^2\right)\right]\\ &-\sum_{\lambda\lambda'}\psi_{\lambda\lambda'}^{\nu\mu}\left(C^1_{\mu\lambda' l'}C^4_{\nu\lambda l}+C^2_{\mu\lambda' l'}C^3_{\nu\lambda l}\right)\Bigg\}\quad\text{for }\chi>0\end{aligned} \tag{43}$$

and

$$\begin{aligned}\int_{B_{\nu\mu}}\left(\frac{\partial\psi}{\partial t}\right)_{\boldsymbol{E}}P_\nu^l P_\mu^{l'}\mathrm{d}\varepsilon\,\mathrm{d}\chi = \alpha_{E^*}\Bigg\{&\frac{2}{\Delta_\varepsilon}\sum_{\lambda\lambda'}C^1_{\mu\lambda' l'}\left[\psi_{\lambda\lambda'}^{\nu\mu}\beta(\varepsilon_\nu)-\psi_{\lambda\lambda'}^{\nu-1\mu}(-1)^l\beta(\varepsilon_{\nu-1})\right]\\ &+\frac{2}{\Delta_\chi}\sum_{\lambda\lambda'}(-1)^{\lambda'}C^3_{\nu\lambda l}\left[\psi_{\lambda\lambda'}^{\nu\mu+1}\left(1-\chi_\mu^2\right)-\psi_{\lambda\lambda'}^{\nu\mu}(-1)^{l'}\left(1-\chi_{\mu-1}^2\right)\right]\\ &-\sum_{\lambda\lambda'}\psi_{\lambda\lambda'}^{\nu\mu}\left(C^1_{\mu\lambda' l'}C^4_{\nu\lambda l}+C^2_{\mu\lambda' l'}C^3_{\nu\lambda l}\right)\Bigg\}\quad\text{for }\chi<0.\end{aligned} \tag{44}$$

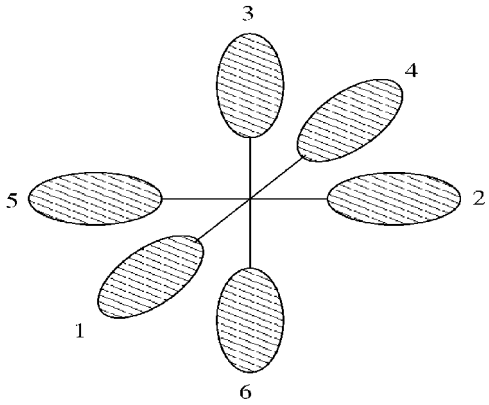

Figure 2. Numbering of the energy valleys.

Here, we have introduced the abbreviations

$$\beta(\varepsilon) = \frac{\gamma^{1/2}}{1 + 2\alpha\varepsilon} \tag{45a}$$

$$C^1_{\mu\lambda' l'} = \int_{-1}^{1} \chi\, P^{\lambda'}(x_\mu) P^{l'}(x_\mu)\, \mathrm{d}x_\mu \tag{45b}$$

$$C^2_{\mu\lambda' l'} = \frac{2}{\Delta_\chi} \int_{-1}^{1} (1 - \chi^2) \frac{\mathrm{d}P^{l'}(x_\mu)}{\mathrm{d}x_\mu} P^{\lambda'}(x_\mu)\, \mathrm{d}x_\mu \tag{45c}$$

$$C^3_{\nu\lambda l} = \int_{-1}^{1} P^{\lambda}(x_\nu) \frac{1}{2\gamma^{1/2}} P^{l}(x_\nu)\, \mathrm{d}x_\nu \tag{45d}$$

$$C^4_{\nu\lambda l} = \frac{2}{\Delta_\varepsilon} \int_{-1}^{1} \beta(\varepsilon) \frac{\mathrm{d}P^{l}(x_\nu)}{\mathrm{d}x_\nu} P^{\lambda}(x_\nu)\, \mathrm{d}x_\nu. \tag{45e}$$

Since all moment equations are linear, it is convenient to rewrite them in matrix form. Therefore, we number the valleys as shown in figure 2 and collect the unknowns $\psi^{(i)\lambda\lambda'}_{\nu\mu}$ in a vector representation $\hat{\psi} = \{\hat{\psi}^1, \ldots, \hat{\psi}^6\}$ with $\hat{\psi}^i = \left\{\psi^{(i)00}_{11}, \ldots, \psi^{(i)\lambda\lambda'}_{\nu\mu}, \ldots, \psi^{(i)\Lambda_\varepsilon\Lambda_\chi}_{N_\varepsilon N_\chi}\right\}$. The system of moment equations now reads

$$\frac{\mathrm{d}}{\mathrm{d}t}\hat{\psi} = \begin{pmatrix} s_1 & f & f & \mathrm{g} & f & f \\ f & s_2 & f & f & \mathrm{g} & f \\ f & f & s_3 & f & f & \mathrm{g} \\ \mathrm{g} & f & f & s_4 & f & f \\ f & \mathrm{g} & f & f & s_5 & f \\ f & f & \mathrm{g} & f & f & s_6 \end{pmatrix} \hat{\psi} = M\hat{\psi} \tag{46}$$

with f and g being matrices describing gain processes due to f- and g-type intervalley scattering, whereas the matrices s_i describe the corresponding loss processes, acoustic intravalley scattering and the impact of the electric field on the valley i. Because the magnitude of the transformed electric field vector $\boldsymbol{E}^{*(i)}$ is equal for opposite valleys, the effect of the electric field is the same for both valleys. Hence, one finds the symmetry $s_4 = s_1$, $s_5 = s_2$ and $s_6 = s_3$.

The steady-state solution to the BTE can now be determined by solving

$$M\hat{\psi} = 0. \tag{47}$$

To find a nontrivial as well as unique solution to equation (47), one must ensure that $\det M = 0$ and $\dim(\mathrm{Ker}\, M) = 1$. The electron density n is a conserved quantity in our physical system. This fact causes a linear dependence of rows in the matrix M, which can be realized in the following way. As already mentioned above, moment equations with the weight $P_\nu^0 P_\mu^0$ can be interpreted as continuity equations for a certain cell $B_{\nu\mu}$. Summation over all cells leads to

$$\sum_{\nu\mu} \frac{\partial n_{\nu\mu}}{\partial t} = \frac{\partial n}{\partial t} \stackrel{!}{=} 0 \tag{48}$$

and since a certain row of M corresponds to $\partial n_{\nu\mu}/\partial t$ equation (48) states nothing else as a linear dependence of rows with all scalar multipliers set equal to 1.

The steady-state solution to the homogeneous system (47) is determined except for a normalization factor, which is found by the condition

$$n = \sum_{i=1}^{6} n^i = \frac{1}{V} \sum_i \sum_{\boldsymbol{k},\uparrow+\downarrow} f^i(\boldsymbol{k}) = \frac{m_d^{3/2}\sqrt{2}}{\hbar^3\pi^2} \sqrt{\Delta_\varepsilon \Delta_\chi} \sum_i \sum_{\nu\mu} \psi_{\nu\mu}^{(i)00} \tag{49}$$

where n^i denotes the particle density of the ith valley. The relevant macroscopic quantities, namely the drift velocity $\boldsymbol{v}_d$ and the mean energy $\langle\varepsilon\rangle$, can now be easily obtained from the distribution function. By using the definition of the group velocity $\boldsymbol{v}_{\boldsymbol{k}}$ of an electron with wavevector $\boldsymbol{k}$,

$$\boldsymbol{v}_{\boldsymbol{k}} = \frac{1}{\hbar} \frac{\partial \varepsilon}{\partial \boldsymbol{k}} \tag{50}$$

the drift velocity in real axis system results in

$$\boldsymbol{v}_d = \frac{1}{nV} \sum_i \sum_{\boldsymbol{k},\uparrow+\downarrow} f^i(\boldsymbol{k}) \boldsymbol{v}_{\boldsymbol{k}} = \frac{1}{nV} \sum_i D_i^{-1} T \{\hat{e}_{E^{*(i)}}\}_p \, j_z^{*(i)} \tag{51}$$

with

$$j_z^{*(i)} = \frac{V m_0}{\pi^2\hbar^3} \left(\frac{m_d}{m_0}\right)^{3/2} \frac{\sqrt{\Delta_\varepsilon \Delta_\chi}}{2} \sum_{\nu\mu} \sum_{\lambda\lambda'} \psi_{\nu\mu}^{(i)\lambda\lambda'} \int_{-1}^{1} \chi P^{\lambda'} \,\mathrm{d}x_\mu \int_{-1}^{1} P^\lambda \beta \,\mathrm{d}x_\nu. \tag{52}$$

Here, D_i^{-1} denotes the inverse transformation matrix between the real axis system and the principal axis system of the ith valley, T is the Herring–Vogt matrix (3) and $\{\hat{e}_{E^{*(i)}}\}_p$ is a unit vector in field direction expressed in the corresponding principal axis system. The mean energy is obtained by

$$\langle\varepsilon\rangle = \frac{1}{nV} \sum_i \sum_{\boldsymbol{k},\uparrow+\downarrow} f^i(\boldsymbol{k}) \varepsilon = \frac{m_d^{3/2}}{n\sqrt{2}\pi^2\hbar^3} \sqrt{\Delta_\chi \Delta_\varepsilon} \sum_i \sum_{\nu\mu\lambda} \psi_{\nu\mu}^{(i)\lambda 0} \int_{-1}^{1} P^\lambda \varepsilon \,\mathrm{d}x_\nu. \tag{53}$$

4. Numerical results

The physical parameters of silicon used in our numerical simulations are listed in table 1. We were advised to use some different deformation potential constants, in particular for acoustic intravalley scattering, as used in the MC calculations of Canali *et al* [22] to find best agreement with experimental data. To keep the numerical calculations both accurate and as fast as possible, we were limited to quadratic matrices up to a dimension of about

Table 1. Physical parameters of silicon used in the numerical simulations.

Quantity	Value	Units	Quantity	Value	Units
m_t/m_0	0.19	–	$\hbar\omega_{2,f}$	47	meV
m_l/m_0	0.916	–	$(D_tK)^2_{2,f}$	2×10^8	eV cm^{-1}
ρ	2.329	g cm^{-3}	$\hbar\omega_{3,f}$	59	meV
α	0.5	1/eV	$(D_tK)^2_{3,f}$	2×10^8	eV cm^{-1}
u_l	9.04×10^5	cm s^{-1}	$\hbar\omega_{1,g}$	12	meV
u_t	5.34×10^5	cm s^{-1}	$(D_tK)^2_{1,g}$	0.9×10^8	eV cm^{-1}
n	10^{13}	1 cm^{-3}	$\hbar\omega_{2,g}$	19	meV
Ξ_1	5.8×10^8	eV	$(D_tK)^2_{2,g}$	1.5×10^8	eV cm^{-1}
$\hbar\omega_{1,f}$	19	meV	$\hbar\omega_{3,g}$	62	meV
$(D_tK)^2_{1,f}$	0.15×10^8	eV cm^{-1}	$(D_tK)^2_{3,g}$	11×10^8	eV cm^{-1}

10 000 due to our computer resources. For the case of a fixed number of unknowns, the numerical results proved to be better if one uses as many cells as possible and to approximate the distribution function only by a constant interpolation within each cell than to perform the simulations with a smaller number of cells and to approximate the distribution function by Legendre polynomials of higher order. Hence, considering the six energy valleys, the χ-space was split into 12 groups, whereas in the energy space a maximum resolution of 150 intervals was used. Since the maximum energy $\varepsilon_{N_\varepsilon}$ (from which onwards the distribution function can be assumed to vanish) increases with the applied field, the energy discretization length Δ_ε was varied from 2 meV for low electric fields (up to 1 kV cm^{-1}) to 20 meV for high electric fields ($\approx$100 kV cm^{-1}). All numerical results obtained for fields higher than 100 kV cm^{-1} must be taken cautiously, because upper energy valleys and the second conduction band, respectively, are not included in our model. For extremely high fields of about 500 kV cm^{-1} the distribution function starts to spread over the whole first Brillouin zone [9] and the concept of separated energy valleys becomes untenable. Moreover, when there is a sufficient amount of electrons with energies higher than the energy gap of silicon ($\approx$1.1 eV), impact ionization becomes an important scattering mechanism.

Figure 3 shows the calculated drift velocity as a function of the electric field applied parallel to $\langle 111 \rangle$ and $\langle 100 \rangle$ directions at liquid nitrogen and room temperature compared to measurements [22] and MC data [21]. Since optical intervalley scattering becomes dominant for high fields, the drift velocity nearly saturates for high enough electric fields. The observed anisotropy of the drift velocity can be explained by the fact that if the electric field is parallel to the $\langle 111 \rangle$ direction, its effect is the same on all six energy valleys, whereas applying it along a $\langle 100 \rangle$ direction, it 'heats' the valleys in a different way. In the latter case, the two valleys with their long principal axes parallel to the electric field become colder than the other four. Intervalley scattering tries to compensate for the 'temperature' differences, which leads to a repopulation between cold and hot valleys. Figure 4 illustrates the dependence of the ratio of the particle densities according to hot and cold valleys on the electric field at $T = 77$ K. For comparison, MC data from Canali *et al* [22], scaling technique results from Holm–Kennedy and Champlin [24] and refractive-index anisotropy measurements of Vorobyov *et al* [25] are also indicated.

The mean electron energy as a function of the electric field applied along $\langle 111 \rangle$ direction at $T = 300$ K and $T = 77$ K compared to MC calculations [21, 22] is shown in figure 5. The MC data obtained from Fischetti and Laux, indicated as circles, are based on an empirical-pseudopotential band structure calculation, whereas Canali *et al* used a simple parabolic six energy valley model in their MC simulations. As expected, we find better agreement with

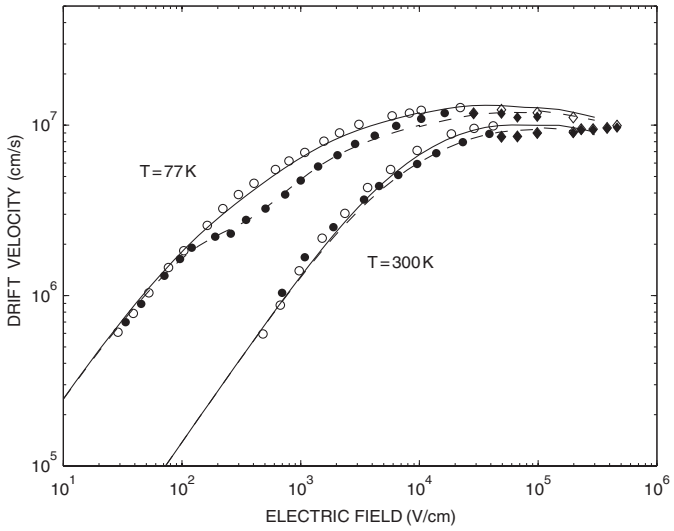

Figure 3. Electron drift velocity as a function of the electric field at a temperature of 77 and 300 K. Open and closed circles refer to experimental data [22] obtained with the field parallel to ⟨111⟩ and ⟨100⟩ directions. A high field extension is given by MC results from Fischetti and Laux [21] indicated by open and closed diamonds again for ⟨111⟩ and ⟨100⟩ directions. Solid and dashed lines show the results obtained by our multicell matrix method.

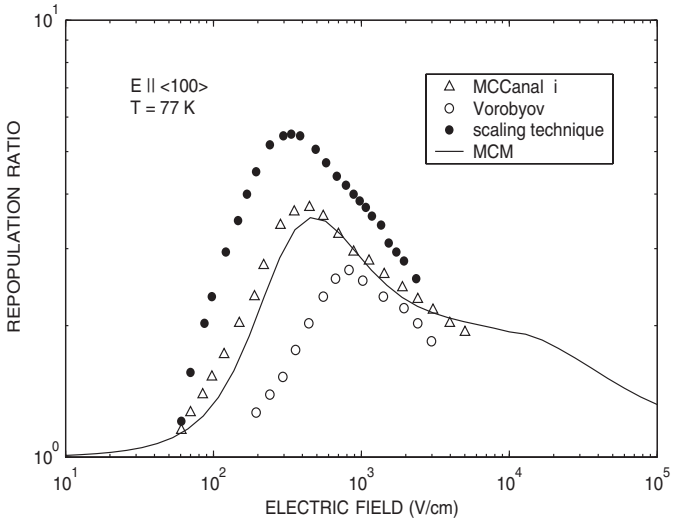

Figure 4. Repopulation ratio of cold-to-hot valley as function of the electric field applied along the ⟨100⟩ direction at $T = 77$ K. Closed and open circles indicate the results in [24] and [25], respectively, whereas triangles indicate MC results from Canali *et al* [22]. The solid line refers to the multicell matrix results (MCM).

data obtained by Canali *et al*, although the mean energy obtained by our multicell method is somewhat lower for high fields.

Applying the electric field along nonsymmetry directions leads to the so-called transversal anisotropy effect, first found by Sasaki and Shibuya in germanium. Here, the resulting

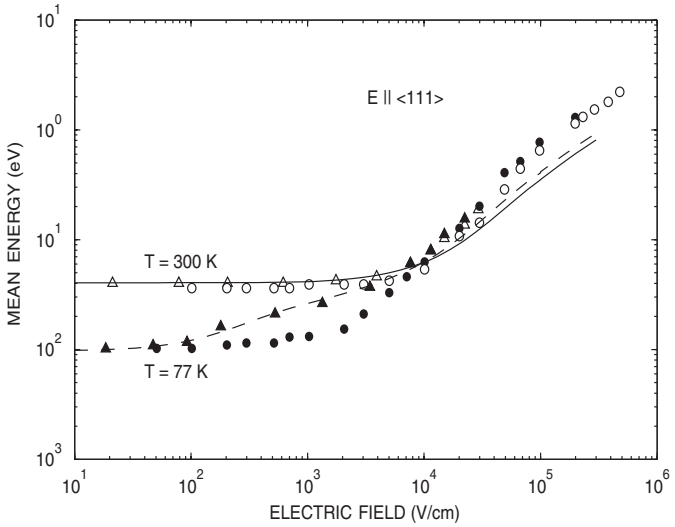

Figure 5. Mean electron energy as function of electric field applied along ⟨111⟩ direction at $T = 77$ K and $T = 300$ K. Triangles and circles indicate MC results obtained from Canali *et al* [22] and Fischetti and Laux [21], respectively. Multicell matrix results refer to solid and dashed lines.

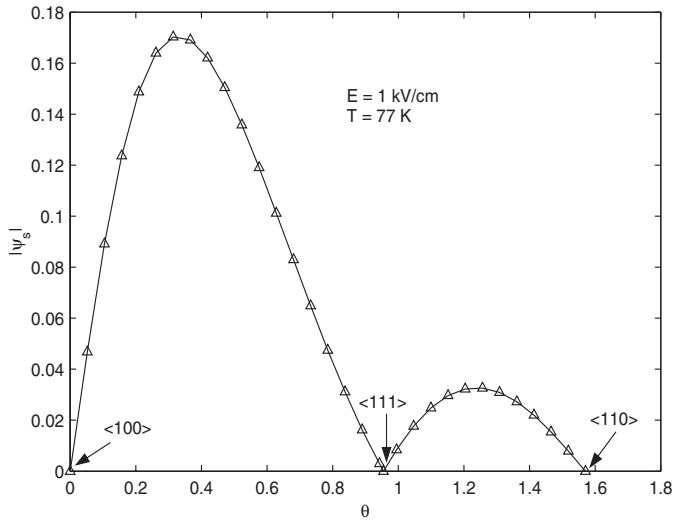

Figure 6. Calculated modulus of the angle ψ_s between field vector and current density at $T = 77$ K when changing the field vector with constant modulus $E = 1$ kV cm^{-1} from ⟨001⟩ over ⟨111⟩ to ⟨110⟩ direction, which is indicated by the polar angle θ.

drift velocity vector is no longer parallel to the electric field vector. Figure 6 shows the calculated angle ψ_s between both vectors at $T = 77$ K when changing continuously the electric field vector from ⟨001⟩ over ⟨111⟩ to ⟨110⟩ direction, which is indicated by a polar angle θ. For the symmetry directions, the angle ψ_s vanishes as expected. Since the number of intervalley phonons increases with temperature, all anisotropy effects decrease with increasing temperatures.

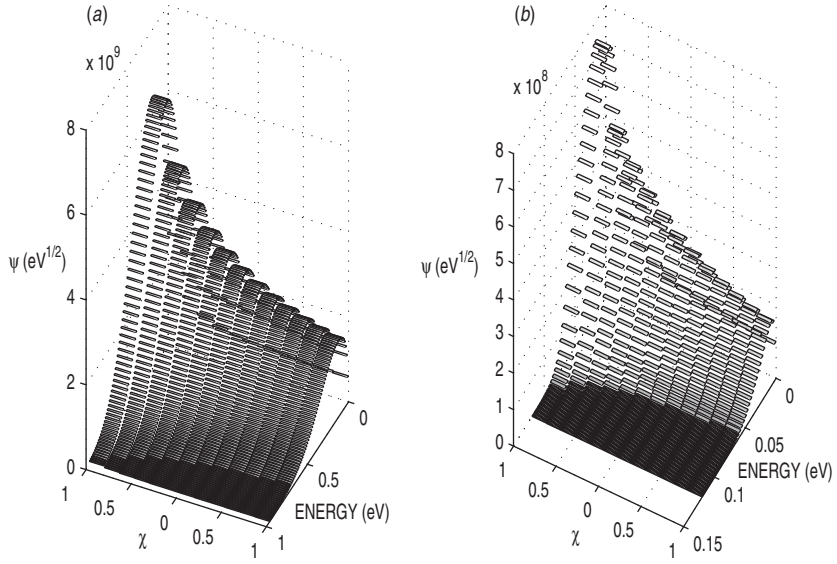

Figure 7. Distribution function ψ versus energy and χ at $T = 77$ K for $E = 60$ kV cm^{-1} (*a*) and $E = 1$ kV cm^{-1} (*b*), respectively. The field was applied along $\langle 111 \rangle$ direction.

Finally, the distribution function according to a certain energy valley is shown in figure 7 for different indicated electric fields at $T = 77$ K. As also known from MC simulations one notices that simple analytical approximations of the distribution function, e.g., a 'drifted' Maxwellian with a free temperature parameter, will be insufficient for high electric fields.

5. Conclusion

In this paper a new multicell matrix method for solving the BTE for the steady-state regime in semiconductors is presented. Its main advantage compared to MC simulations is the low cost of CPU time. The method is tested for a simplified model including only the lowest energy valleys of n-type silicon. The comparison of numerical results to experimental and MC data shows that the model is applicable up to fields of about 60 kV cm^{-1}. For higher fields it will be necessary to consider a more detailed band structure and the impact ionization of electrons.

Acknowledgments

This work was supported by the Fonds zur Förderung der wissenschaftlichen Forschung, Vienna, under contract number P14669-TPH.

References

[1] Duderstadt J and Martin W 1979 *Transport Theory* (New York: Wiley)
[2] Caraffini G L, Ganapol B D and Spiga G 1995 A multigroup approach to the non-linear extended Boltzmann equation *Nuovo Cimento* D **17** 129
[3] Rossani A and Spiga G 1998 Kinetic theory with inelastic interactions *Transp. Theory. Stat. Phys.* **27** 261
[4] Koller W 2000 *Semi-continuous and multigroup models in extended kinetic theory PhD Thesis* Technical University, Graz 135

[5] Ertler C and Schürrer F 2002 A multigroup spline approximation in extended kinetic theory *J. Phys. A: Math. Gen.* **35** 8673
[6] Bell G and Glasstone S 1970 *Nuclear Reactor Theory* (New York: Van Nostrand Reinhold)
[7] Lapidus L and Pinder G F 1982 *Numerical Solution of Partial Differential Equations in Science and Engineering* (New York: Wiley)
[8] Majorana A 1991 Space homogeneous solutions of the Boltzmann equation describing electron phonon interactions in semiconductors *Transp. Theory. Stat. Phys.* **20** 261
[9] Kunikiyo T, Takenaka M, Kamakura Y, Yamaji M, Mizuno H, Morifuji M, Taniguchi K and Hamaguchi C 1994 A Monte Carlo simulation of anisotropic electron transport in silicon including full band structure and anisotropic impact-ionization model *J. Appl. Phys.* **75** 297
[10] Fischetti M V 1991 Monte Carlo simulation of transport in technologically significant semiconductors of the diamond and zinc-blende structures. Part I: homogeneous transport *IEEE Trans. Electron. Devices* **38** 634
[11] Budd H 1966 *Proc. Int. Conf. on the Physics of Semiconductors (Kyoto) J. Phys. Soc. Japan Suppl.* **21** 420
[12] Nougier J P and Rolland M 1973 Mobility, noise temperature and diffusivity of hot holes in germanium *Phys. Rev.* B **8** 5728
[13] Alam M A, Stettler M S and Lundstrom M S 1993 Formulation of the Boltzmann equation in terms of scattering matrices *Solid-State Electron.* **36** 263
[14] Aubert J P, Vaissiere J C and Nougier J P 1984 Matrix determination of the stationary solution of the Boltzmann equation for hot carriers in semiconductors *J. Appl. Phys.* **56** 1128
[15] Fatemi E and Odeh F 1993 Upwind finite difference solution of Boltzmann equation applied to electron transport in semiconductor devices *J. Comput. Phys.* **108** 209
[16] Majorana A and Pidatella R M 2001 A finite difference scheme solving the Boltzmann-Poisson system for semiconductor devices *J. Comput. Phys.* **174** 649
[17] Jacoboni C and Reggiani L 1983 The Monte Carlo method for the solution of charge transport in semiconductors with application to covalent materials *Rev. Mod. Phys.* **55** 645
[18] Herring C and Vogt E 1956 Transport and deformation-potential theory for many-valley semiconductors with anisotropic scattering *Phys. Rev.* **101** 944
[19] Streitwolf H W 1970 *Phys. Status Solidi* B **37** K47
[20] Lax M and Birman J L 1972 *Phys. Status Solidi* B **49** K153
[21] Fischetti M V and Laux S E 1988 Monte Carlo analysis of electron transport in small semiconductor devices including band-structure and space-charge effects *Phys. Rev.* B **38** 9721
[22] Canali C, Jacoboni C, Nava F, Ottaviani G and Alberigi-Quaranta A 1975 Electron drift velocity in silicon *Phys. Rev.* B **12** 2265
[23] Conwell E M 1967 *High Field Transport in Semiconductors* (Oxford: Academic)
[24] Holm-Kennedy J W and Champlin K S 1970 *Appl. Phys. Lett.* **16** 46
[25] Vorobyov L E, Stafeev V I and Ushakov A U 1973 *Phys. Tech. Semicond.* **7** 919